

## Driven Dynamic Mode Splitting of the Magnetic Vortex Translational Resonance

K. S. Buchanan,<sup>1,\*</sup> M. Grimsditch,<sup>2</sup> F. Y. Fradin,<sup>2</sup> S. D. Bader,<sup>1,2</sup> and V. Novosad<sup>2</sup>

<sup>1</sup>Center for Nanoscale Materials, Argonne National Laboratory, Argonne, Illinois 60439, USA

<sup>2</sup>Materials Science Division, Argonne National Laboratory, Argonne, Illinois 60439, USA

(Received 10 April 2007; revised manuscript received 16 August 2007; published 27 December 2007)

A magnetic vortex in a restricted geometry possesses a nondegenerate translational excitation that corresponds to circular motion of its core at a characteristic frequency. For 40-nm thick, micron-sized permalloy elements, we find that the translational-mode microwave absorption peak splits into two peaks that differ in frequency by up to 25% as the driving field is increased. An analysis of micromagnetic equations shows that for large driving fields two stable solutions emerge.

DOI: [10.1103/PhysRevLett.99.267201](https://doi.org/10.1103/PhysRevLett.99.267201)

PACS numbers: 75.40.Gb, 75.30.Ds, 75.75.+a

Nonlinear phenomena are ubiquitous in nature, existing in systems ranging from leaky faucets to atmospheric circulation to optics [1–3]. Magnetic systems can be models for improving our understanding of nonlinear phenomena since they are experimentally accessible and the equations of motion are generally tractable. In magnetism, nonlinear effects were first observed in high-power ferromagnetic resonance experiments in the 1950s [4,5] where the premature saturation of the main absorption peak and the emergence of subsidiary peaks were attributed to spin-wave generation [6]. These initial nonlinear dynamic studies focused on a saturated magnetic state. More recently, magnetic systems have been shown to exhibit a wealth of other interesting phenomena, such as spin-wave self-focusing [7], symmetry breaking spin-wave Möbius solitons [8], and foldover and bistability effects [9].

The spin vortex state, an in-plane flux-closure magnetization distribution with a small central core, is often observed in magnetically soft microstructures [10–12]. Spin-polarized scanning tunneling microscopy shows that the core radius is  $\sim 10$  nm, comparable to the material's exchange length [13]. Because of the Magnus-type force (gyroforce) that acts on the core, magnetic vortices exhibit unique dynamic excitations, including the translational or gyrotropic mode that is characterized by sub-GHz, spiral-like core motion [14–20], distinct from the higher frequency (GHz range) quantized spin waves observed in restricted geometries [21–23]. The core polarization  $p = \pm 1$  determines the handedness of the spiral motion, as demonstrated by time-resolved magneto-optical Kerr [24–26] and x-ray experiments [27]; the restoring force is provided mainly by the magnetostatic energy [16,28].

Here we explore frequency- and amplitude-dependent dynamics of magnetic vortices in circular and elliptical microdisks excited by a radio frequency (rf) driving field. We find that as the magnitude of the rf field  $h_{ac}$  is increased, the resonance peak corresponding to the vortex translational mode splits into two well-defined peaks whose separation increases with  $h_{ac}$ . The appearance of mode splitting is unusual since for a single dot this is a

nondegenerate mode. (There is a degeneracy in the sense that the ensemble contains random chiralities and polarities with the same eigenfrequency but we find no indication in simulations that their high-field response should differ.) However, comparing the results with micromagnetic calculations and a phenomenological analytical model reveals that this system is similar to a driven anharmonic oscillator where a nonlinear energy potential can lead to two resonance states, thereby resolving the apparent contradiction of a split, nondegenerate mode. Nevertheless, the prevailing theory for magnetic vortex dynamics does not fully explain our observations.

We use a microwave reflection technique to investigate the excitations of vortices in magnetic microstructures [29]. Elliptical and circular permalloy (Fe<sub>20</sub>Ni<sub>80</sub> alloy) microdisks were patterned on the central strip of coplanar waveguides (CPW),  $\sim 2000$  per waveguide separated by  $>1$   $\mu\text{m}$  to minimize dipolar interactions, using  $e$ -beam lithography and liftoff. A rf current in the waveguide generates an in-plane rf magnetic field that is preferentially absorbed when the frequency coincides with a resonance. The derivatives of the CPW impedance are recorded with respect to a small modulation field applied parallel to the static, in-plane magnetic field  $H$ , and  $h_{ac}$  is calculated from the current in the CPW. We examine three samples:  $2.2 \times 1.1$   $\mu\text{m}$  ellipses,  $3.1 \times 1.7$   $\mu\text{m}$  ellipses, and circles of diameter  $2.2$   $\mu\text{m}$ , all 40-nm thick, referred to as samples  $A$ ,  $B$ , and  $C$ , respectively. All are in the single-vortex ground state with a mixture of chiralities and polarities.

Figure 1(a) shows microwave impedance spectra as a function of  $h_{ac}$  for sample  $A$  with  $H = 60$  Oe along the ellipse minor axis, orthogonal to  $h_{ac}$ . Magneto-optical Kerr effect measurements (not shown) indicate that this is below the vortex annihilation field of 2.5 kOe along the minor (hard) axis. A single, symmetric peak is found at  $\sim 130$  MHz for low  $h_{ac}$ . As  $h_{ac}$  is increased, it broadens and develops a shoulder ( $h_{ac} \sim 11$  Oe) and then splits into two, where one branch increases in frequency and the other decreases, reaching a separation of 40 MHz for  $h_{ac} \sim 24$  Oe. Figure 1(b) shows how the microwave spectra

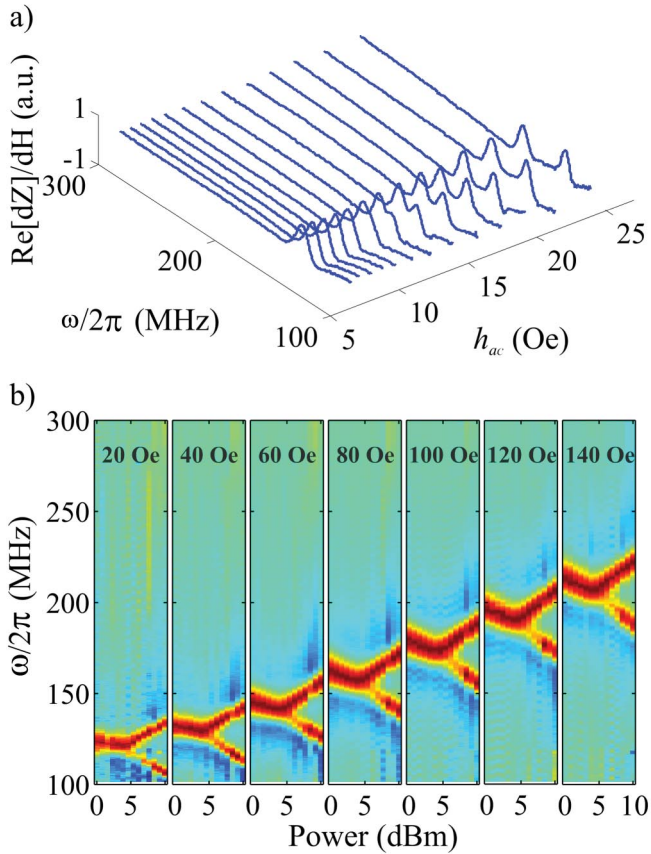


FIG. 1 (color online). (a) Microwave spectra (real part, scaled) for sample A,  $H = 60$  Oe, as a function of  $h_{ac}$ . (b) Spectra showing dynamic splitting as a function of excitation power for  $H = 20$ – $140$  Oe applied along the ellipse minor axis.

change as a function of  $H$ . Spectra at  $H = 0$  Oe, obtained using background subtraction (not shown), are similar to those obtained at  $H = 20$  Oe. The increase in resonance frequency with  $H$  is related to the increasing curvature of the energy profile, as described in [28]. Both the critical  $h_{ac}$  and the splitting magnitudes, however, are relatively insensitive to  $H$ . The frequencies below the critical  $h_{ac}$  vary little for small  $H$  but take on a negative slope for larger  $H$ , which may be related to the asymmetry of the energy profile of the shifted vortex [28].

The data for sample B (not shown) are similar except the frequencies are lower ( $\sim 80$  MHz for  $H = 20$  Oe) due to the smaller aspect ratio [11]. Splitting begins at  $h_{ac} \sim 7$  Oe along the major axis, reaches 21 MHz at  $h_{ac} \sim 10$  Oe, and changes little with  $H$ . The critical  $h_{ac}$  is slightly higher when directed along the ellipse minor axis. For circular dots (sample C), splitting effects were detected at  $h_{ac}$  of only 3.6 Oe and the splitting reaches 17 MHz at  $h_{ac} \sim 5.5$  Oe. The vortex translational-mode splitting is thus observed at large  $h_{ac}$  (*nonlinear regime*) for all measured samples and is relatively insensitive to  $H$ .

Since the vortex translational mode is nondegenerate, the key question is, Why is mode splitting observed?

To explore this further, we use micromagnetic theory and computation, both of which are in excellent agreement with experiments for small  $h_{ac}$  (*linear regime*) [18,21,24,26,27,30]. We include additional terms in Thiele's equation [14] to describe the nonlinear demagnetization and Zeeman energy profiles expected at higher  $h_{ac}$  and we use micromagnetic simulations to model the effect of increasing  $h_{ac}$ . In spite of incomplete agreement with experiment, both approaches show evidence for the emergence of two allowed modes at high  $h_{ac}$ , only one of which is accessed at a given time.

Thiele's equation  $-\mathbf{G} \times \frac{d\mathbf{X}}{dt} - D \frac{d\mathbf{X}}{dt} + \frac{\partial W(\mathbf{X})}{\partial \mathbf{X}} = 0$  describes the motion of the vortex core position  $\mathbf{X} = (X, Y)$  in a phenomenological energy well  $W(\mathbf{X})$ , where  $t$  is time and  $D$  is a damping parameter [30]. The gyrovector  $\mathbf{G} = -Gp\hat{z}$  induces the spiral motion of the core, where  $G = 2\pi LM_s/\gamma$ ,  $\gamma$  is the gyromagnetic ratio, and  $M_s$  is the saturation magnetization [24–26].  $W(\mathbf{X})$  provides the restoring force. The dipolar portion of  $W$ ,  $W_{dem}$ , is quadratic for small amplitudes, leading to harmonic-oscillator-like equations of motion. For large displacements, higher order terms must be included [28], leading to equations of motion similar to those describing an anharmonic oscillator. Considering contributions up to 4th order in  $\mathbf{X}$ ,  $W_{dem}(\mathbf{X}) = (\kappa/2)\mathbf{X}^2 + (\beta/4)\mathbf{X}^4$  for a circular disk. The Zeeman energy is  $W_Z = -\mathbf{M} \cdot \mathbf{h}$ , where  $\mathbf{h} = h_{ac} \sin(\omega t)\hat{t}$  is the driving magnetic field at frequency  $\omega$ . For small  $\mathbf{X}$ ,  $M_x \propto Y$ , but the general form is  $M_x = C_1 Y + C_2 Y(Y^2 + X^2)$ , where  $C_1$ , and  $C_2$  are adjustable parameters. For  $\beta = C_2 = 0$ , the eigenfrequency is  $\omega_0 = G^{-1}\sqrt{\kappa}$  [16]. Damping effects may also contribute [31], but should primarily affect the amplitude and width of the resonance line.

Figure 2 shows numerical solutions calculated using the parameters of sample C [32] assuming a solution of the form  $\mathbf{X} = A_x \cos(\omega t + \phi)\hat{i} + A_y \sin(\omega t + \phi)\hat{j}$ , where  $A_x$  and  $A_y$  represent the amplitudes of the core motion along  $x$  and  $y$  and  $\phi$  is the phase lag between  $h_{ac}$  and the vortex response.  $\beta$  was chosen to provide a small narrowing of

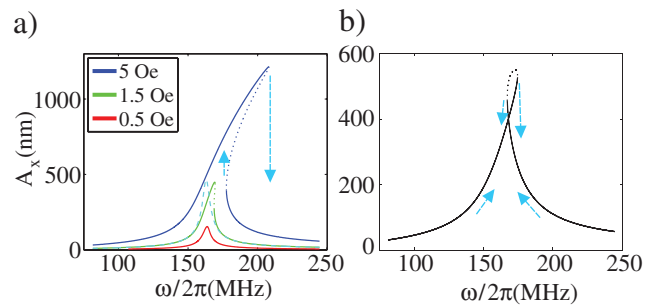


FIG. 2 (color online). (a) Calculated vortex core motion amplitude as a function of  $\omega$  for a circular disk with  $\beta > 0$  shows a foldover effect when  $h_{ac}$  (values in legend) is increased. Arrows indicate the hysteric path and the dashed line shows the  $\beta = 0$  result for  $h_{ac} = 1.5$  Oe. (b)  $A_x$  vs  $\omega/2\pi$  using a large  $C_2$  value shows a crossover effect for  $h_{ac} = 5$  Oe.

$W_{\text{dem}}(\mathbf{X})$ , and  $C_1 \sim M_s V/R$ , where  $V$  is the volume, estimated by assuming that the vortex annihilation approximately corresponds to saturation. We also considered 3rd harmonics but found they are suppressed by several orders of magnitude. As the driving field is increased a foldover of the solution is observed, as reported previously for nonlinear oscillators [33], high-power ferromagnetic resonators [34], and in nonlinear optics [2]. The solution changes little for small  $C_2$  ( $C_2 = C_3 = -0.1C_1/R^2$ , considered reasonable based on fits to  $M$  vs  $X$  from micromagnetic simulations), but for larger  $C_2 = -2.5C_1/R^2$  crossover behavior is found [Fig. 2(b)]. Both solutions lead to two peaks, as indicated by arrows in Fig. 2. Figure 2(a) shows both frequencies increasing as  $h_{\text{ac}}$  is increased, whereas Fig. 2(b) is qualitatively closer to the experimental trends as it allows for one peak to increase with  $h_{\text{ac}}$  while the other decreases. Note, however, that the value of  $C_2$  used in Fig. 2(b) is larger than can be justified based on simulations.

Micromagnetic modeling was conducted based on the Landau-Lifshitz-Gilbert equation [35]. To achieve tractable computational times ( $\sim 3$  days on a workstation), a scaled-down ellipse with dimensions  $300 \times 150$  nm, 20-nm thick, of permalloy [32] was used with  $3 \times 3$  nm<sup>2</sup> cells. A sinusoidal driving magnetic field  $h(t) = h_{\text{ac}} \sin(\omega t)$  was applied parallel to the ellipse major axis ( $x$ ) and  $\omega$  was swept slowly to maintain steady-state motion.

Micromagnetic modeling results for  $h_{\text{ac}} = 0.1, 10,$  and  $20$  Oe are shown in Fig. 3. The amplitude  $M_x$  builds and then declines as the frequency is swept through resonance [Fig. 3(a)] and  $\phi$  is zero for low  $\omega$ ,  $\pi$  at high, and passes through  $\pi/2$  at resonance. Since the absorption measured experimentally is proportional to  $M_x \sin(\phi)$ , this effectively decreases the peak widths in Fig. 3 so that they more closely resemble Fig. 1. The forward and reverse sweeps coincide when  $h_{\text{ac}}$  is 0.1 Oe ( $< 1$  MHz difference is due to sweeping). At  $h_{\text{ac}} = 10$  Oe,  $M_x$  builds more slowly and the response is hysteretic, falling off at 637 MHz on the forward sweep and building at 628 MHz on the reverse. At  $h_{\text{ac}} = 20$  Oe the effect is more pronounced (builds at 670 and falls at 643 MHz). Simulations at constant  $\omega = 632$  MHz and  $h_{\text{ac}} = 10$  Oe show that varying the initial phase of the driving field allows two steady-state resonances to be accessed ( $M_x/M_s = 0.127$ ,  $\phi = 2.60$ ;  $M_x/M_s = 0.216$ ,  $\phi = 2.07$ ), confirming that the bistability in Fig. 3 is a steady-state phenomenon. There is no indication from theory or simulations that vortices with different chirality or polarity, other than their direction of core circulation, should behave differently. In the experiment, the frequency is increased in discrete steps and the foldover dependence on sweep direction cannot be detected. Since we are averaging several spectra for many dots we expect that the signal should reflect both bistable states. The magnitude of  $h_{\text{ac}}$  and the separation of the frequency resonance edges in Fig. 3 are

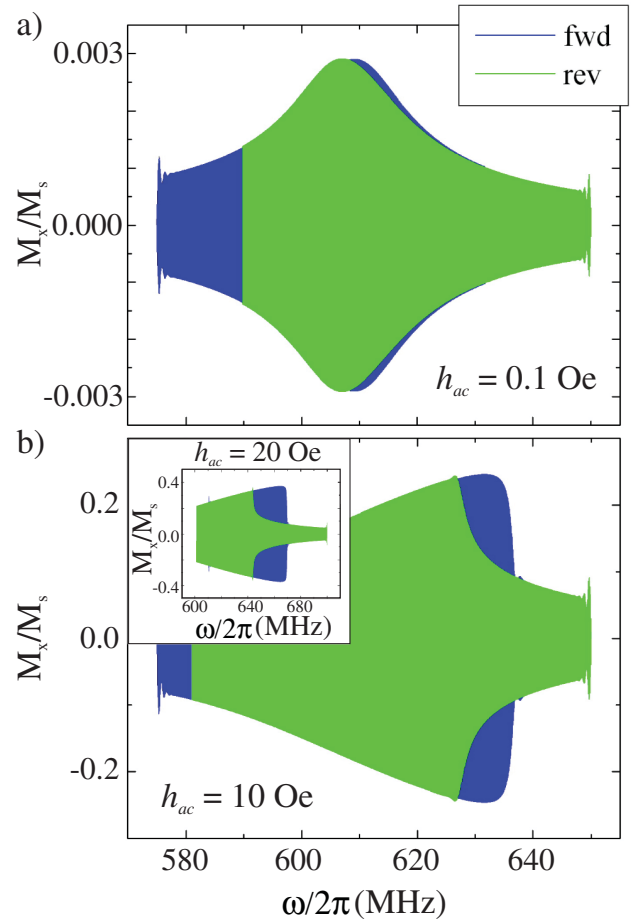


FIG. 3 (color online). Micromagnetic simulations for a  $300 \times 150$  nm ellipse, 20-nm thick, for  $h_{\text{ac}}$  of (a) 0.1 Oe, (b) 10 Oe, and inset of (b) 20 Oe. The frequency was increased [dark (blue)] or decreased [light (green)] at 31.8 kHz/ns, and the  $x$  axis converted from time to  $\omega/2\pi$ .

qualitatively similar to the experiment and they display a foldover effect similar to Fig. 2(a). Assuming comparable representation of the bistable resonances, the expected line shape resembles a peak with a shoulder, as shown for  $h_{\text{ac}} \sim 11$ – $15$  Oe in Fig. 1(a) and not the well-separated peaks observed for larger  $h_{\text{ac}}$ .

For higher  $h_{\text{ac}} = 50$  Oe, the simulations show that the core becomes unstable and will undergo repeated polarization reversal events. For  $\omega$  above and below resonance, steady-state solutions are obtained; however, for a range of  $\omega$  near resonance the amplitude repeatedly builds, declines after the core reversal, and rebuilds, which would lead to a region of decreased absorption in our experiment. Experimental evidence of core flipping by an in-plane rf field has been shown recently [36], which may occur in our samples for the largest  $h_{\text{ac}}$ ; however, micromagnetic modeling and theory indicate that the onset of nonlinear behavior should occur at lower  $h_{\text{ac}}$ .

In summary, using a microwave reflection technique we find that driven magnetic vortices exhibit a nonlinear re-

sponse at the vortex translational-mode resonance. For large driving fields we detect a splitting of the translational mode that is surprising since this mode is nondegenerate. Theory and micromagnetic modeling indicate that a foldover-type effect plays a role in defining this behavior and suggest that the two peaks in the absorption spectra correspond to two steady-state solutions that differ in their phase lag relative to the driving field.

We thank K. Yu. Guslienko, A. Slavin, and P. Roy for stimulating discussions. Work at Argonne, including use of the Center for Nanoscale Materials, was supported by the U.S. Department of Energy, Basic Energy Sciences, under Contract No. DE-AC02-06CH11357.

\*Corresponding author.

buchanan@anl.gov

- [1] *Nonlinear Phenomena and Chaos in Magnetic Materials*, edited by P. E. Wigen (World Scientific, River Edge, NJ, 1994), p. 248.
- [2] R. W. Boyd, *Nonlinear Optics* (Academic, New York, 2002), 2nd ed., p. 576.
- [3] J. S. Russell, *Report on Waves, Report of the Fourteenth Meeting of the British Association for the Advancement of Science* (John Murray, London, 1844), pp. 311–390.
- [4] R. W. Damon, *Rev. Mod. Phys.* **25**, 239 (1953).
- [5] N. Bloomberg and S. Wang, *Phys. Rev.* **93**, 72 (1954).
- [6] H. Suhl, *J. Phys. Chem. Solids* **1**, 209 (1957).
- [7] M. Bauer, O. Büttner, S. O. Demokritov, B. Hillebrands, V. Grimalsky, Yu. Rapoport, and A. N. Slavin, *Phys. Rev. Lett.* **81**, 3769 (1998).
- [8] S. O. Demokritov, A. A. Serga, V. E. Demidov, B. Hillebrands, M. P. Kostylev, and B. A. Kalinikos, *Nature (London)* **426**, 159 (2003).
- [9] Yu. K. Fetisov and C. E. Patton, *IEEE Trans. Magn.* **40**, 473 (2004).
- [10] T. Shinjo, T. Okuno, R. Hassdorf, K. Shigeto, and T. Ono, *Science* **289**, 930 (2000).
- [11] K. Yu. Guslienko, V. Novosad, Y. Otani, H. Shima, and K. Fukamichi, *Phys. Rev. B* **65**, 024414 (2001).
- [12] R. P. Cowburn, D. K. Koltsov, A. O. Adeyeye, M. E. Welland, and D. M. Tricker, *Phys. Rev. Lett.* **83**, 1042 (1999).
- [13] A. Wachowiak, J. Wiebe, M. Bode, O. Pietzsch, M. Morgenstern, and R. Wiesendanger, *Science* **298**, 577 (2002).
- [14] A. A. Thiele, *Phys. Rev. Lett.* **30**, 230 (1973).
- [15] D. L. Huber, *Phys. Rev. B* **26**, 3758 (1982).
- [16] K. Yu. Guslienko, B. A. Ivanov, V. Novosad, H. Shima, Y. Otani, and K. Fukamichi, *J. Appl. Phys.* **91**, 8037 (2002).
- [17] N. A. Usov and L. G. Kurkina, *J. Magn. Magn. Mater.* **242**, 1005 (2002).
- [18] B. A. Ivanov and C. E. Zaspel, *Phys. Rev. Lett.* **94**, 027205 (2005).
- [19] K. S. Buchanan, P. E. Roy, M. Grimsditch, F. Y. Fradin, K. Yu. Guslienko, S. D. Bader, and V. Novosad, *Nature Phys.* **1**, 172 (2005).
- [20] J. Shibata, Y. Nakatani, G. Tatara, H. Kohno, and Y. Otani, *Phys. Rev. B* **73**, 020403(R) (2006).
- [21] V. Novosad, M. Grimsditch, K. Yu. Guslienko, P. Vavassori, Y. Otani, and S. D. Bader, *Phys. Rev. B* **66**, 052407 (2002).
- [22] L. Giovannini, F. Montoncello, F. Nizzoli, G. Gubbiotti, G. Carlotti, T. Okuno, T. Shinjo, and M. Grimsditch, *Phys. Rev. B* **70**, 172404 (2004).
- [23] B. Hillebrands and K. Ounadjela, *Spin Dynamics in Confined Magnetic Structures I*, Topics in Applied Physics Vol. 83 (Springer, Berlin, 2002).
- [24] J. P. Park, P. Eames, D. M. Engebretson, J. Berezovsky, and P. A. Crowell, *Phys. Rev. B* **67**, 020403 (2003).
- [25] M. Buess *et al.*, *Phys. Rev. Lett.* **93**, 077207 (2004).
- [26] C. E. Zaspel, B. A. Ivanov, J. P. Park, and P. A. Crowell, *Phys. Rev. B* **72**, 024427 (2005).
- [27] S.-B. Choe, Y. Acreman, A. Scholl, A. Bauer, A. Doran, J. Stöhr, and H. A. Padmore, *Science* **304**, 420 (2004).
- [28] K. S. Buchanan, P. E. Roy, M. Grimsditch, F. Y. Fradin, K. Yu. Guslienko, S. D. Bader, and V. Novosad, *Phys. Rev. B* **74**, 064404 (2006).
- [29] V. Novosad, F. Y. Fradin, P. E. Roy, K. Buchanan, K. Yu. Guslienko, and S. D. Bader, *Phys. Rev. B* **72**, 024455 (2005).
- [30] K. Yu. Guslienko, *Appl. Phys. Lett.* **89**, 022510 (2006).
- [31] V. S. Tiberkevich and A. N. Slavin, *Phys. Rev. B* **75**, 014440 (2007).
- [32]  $2R = 1100$  nm,  $L = 40$  nm;  $M_s = 800$  emu/cm<sup>3</sup>; exchange constant  $A_{ex} = 1.3$   $\mu$ erg/cm; no anisotropy;  $\gamma/(2\pi) = 2.83$  MHz/Oe;  $\alpha = 0.01$ ;  $\omega_0/2\pi = 163$  MHz;  $\kappa = G\omega_0/\pi$ ;  $\beta = (3 \times 10^8 \text{ cm}^{-2})\kappa$ ; and  $D$  was calculated as per Ref. [30].
- [33] L. D. Landau and E. M. Lifshitz, *Mechanics* (Pergamon, New York, 1976), 3rd ed., p. 169.
- [34] Y. K. Fetisov and A. V. Makovkin, *Tech. Phys.* **46**, 84 (2001).
- [35] M. J. Donahue and D. G. Porter, *OOMMF User's Guide, Version 1.0* (National Institute of Standards and Technology, Gaithersburg, MD, 1999).
- [36] B. Van Waeyenberge *et al.*, *Nature (London)* **444**, 461 (2006).